6.0

Liquid Simulations & Properties of Butanone & 3-Hexanone

Guido Putignano[a], Lorenzo Tarricone[a]

[a] *Department of Biosystems Science and Engineering, ETH Zürich, Basel, Switzerland*

Abstract

Liquid state plays a crucial role in classical molecular simulations given that most (bio)chemical processes happen in this state. However, while gas and solid states are usually well-described in terms of approximate analytical theories, it's not the same for liquids. Because of that, (bio)chemical processes can be mostly possible through simulations. For this reason, the purpose of this paper is to compare Butanone and 3-Hexanone in liquids. After having created the molecular topology and the initial coordinates, we ran the simulation focusing on pre-equilibration, NPT and NVT. Later, we ran the analysis focusing on Density, Heat Vaporisation, Molar Isochoric Heat Capacity and Radial Distribution Function Coordination Number. We found that computational values tend to be similar to experimental values, expect for the Molar Isochoric Heat Capacity Moreover, butanone has a higher diffusion coefficient and Static Dieletric Permitivity than 3-Hexanone, while it has a lower Heat of Vaporization. With more precise density measures in Butanone than 3-Hexanone, while losing precision in Heat of Vaporization. With this paper, we aim to improve the understanding of reactions in the liquid state, to foster future research in the area.
In order to ease the correction, the report follows the structure of the questions A to F provided in the exercise sheet, while the thinking questions are inserted in their relevant position and clearly marked with **TF**

Keywords: Liquid State, Ketones, Simulation, Biomolecular Systems.

1. Simulations

Simulating a system is important to understand how it may react to find an easy and potentially fast approach to study a biochemical process that would be hard to study in other ways. Especially with liquid, many of the biochemical processes happen in that state.

1.1. Topology

Ketones are a class of organic compounds characterised by the presence of a carbonyl group (a carbon-oxygen double bond, C=O) bonded to two carbon atoms within a hydrocarbon chain. The general chemical formula for a ketone is R1(C=O)R2, where R1 and R2 represent alkyl or aryl groups.

In simpler terms, a ketone can be visualised as a carbon chain with a double-bonded oxygen atom in the middle, and each side of the oxygen is connected to a carbon group. The carbon groups can be part of longer hydrocarbon chains or aromatic rings.

The carbonyl group in a ketone is planar, and the carbon atom in the carbonyl group is sp2 hybridised, which means it forms three sigma bonds with other atoms and has a p orbital available for pi bonding with the oxygen atom. The geometry around the carbon in the carbonyl group is trigonal planar. This report aims mostly to describe Butanone and 3-Hexanone.

Butanone (btn):

- Chemical Formula: $CH_3(CO)CH_2CH_3$
- Common Name: Butanone or Methyl Ethyl Ketone (MEK)
- Structure: $CH_3 - CO - CH_2 - CH_3$
- IUPAC Name: 2-butanone

3-Hexanone (3hn):

- Chemical Formula: $CH_3(CO)CH_2CH_2CH_2CH_3$
- Common Name: 3-Hexanone
- Structure: $CH_3 - CO - CH_2 - CH_2 - CH_2 - CH_3$
- IUPAC Name: 3-hexanone

The first activity of the report focused on simulating results. To make it possible, the creation of the topology was needed, extending it later to 512 molecules

Figure 1: Representation of ketones Butanone & 3-Hexanone

1.2. Energy Minimisation

Energy minimization is a computational technique widely used in various scientific fields, particularly in molecular dynamics simulations, structural biology, and materials science. The goal of energy minimization is to find the most stable configuration of a system by adjusting the positions of its components to minimize the overall energy. In our case, relaxing the strains and bad atom overlaps can be helpful. It was useful setting up some particular parameters

(a) Table 1 Describing PARILIST block for btn

Algorithm	NSNB	RCUTP	RCUTL	SIZE
1	5	0.8	1.4	0.4

(b) Table 2

Algorithm	NSNB	RCUTP	RCUTL	SIZE
1	5	0.8	1.4	0.4

Figure 2: PAIRLIST Parameters

(a) Table 1

NLRELE	APPAK	RCRF	EPSRF	NSLFEXCL
1	0	1.4	17.7	1

(b) Table 2

NLRELE	APPAK	RCRF	EPSRF	NSLFEXCL
2	2	0	1.5	18.0

Figure 3: Parameters Set 2

Compared to other works in the field [1][2], Energy minimisation has been done only once. The reason was mostly due to the size of the molecules. As our molecules were just composed of a few atoms, having the energy minimisation in the vacuum would have been pointless.

1.3. Pre-Equilibration

Before starting our simulations, it's possible to have equilibration processes widely described in previous reports. That can be helpful to equilibrate the system so that is looses the memory of the initial random configuration and velocities. Equlibration can be possible to run at constant volume (NVT) or at constant pressure (NPT).

1.3.1. NPT Simulations

The first step includes a simulation of the system at constant pressure. That was possible at a temperature of 300 K and a pressure of 1 bar to match the thermodynamic standard conditions. In this case, the tables were already filled, but it was important to check if results were correct. In our case, we considered successive 50 jobs.

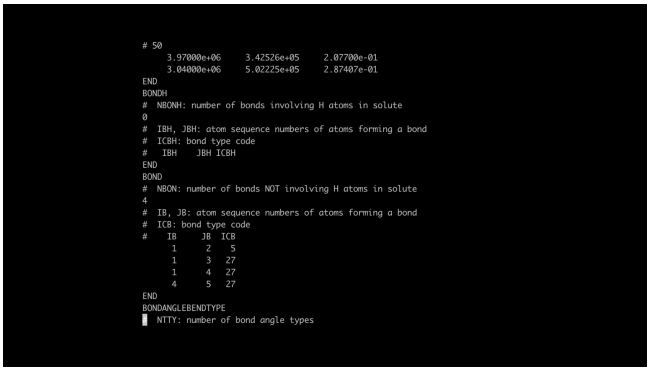

Figure 4: Description of Pressure

1.3.2. NVT Simulations

NVT simulation included the study of the system at 290, 300 and 310 K. To determine the heat capacity at a volume aligned with the equilibrium density of the liquid model at 300 K and 1 bar, we will initiate a separate set of calculations immediately following the 50th job of the preceding NPT calculations. By this point, the box volume should have significantly stabilized, reaching the desired equilibrium value.

2. Analysis

The analysis consisted on the plot of Density, Heat of Vaporisation, Molar Isochoric Heat Capacity, Radial Distribution Function and Coordination Number, Static Dieletric Permitivity and Self-Diffusion Coefficient

2.1. Density

The first part of the analysis included calculating The equilibrium box volume, density, total energy and total potential energy of the two ketones.

Equilibrium Box Volume

- **Description:** The volume of the simulation box containing the molecular system.
- **Importance:** Determines system density and reveals spatial distribution of molecules. Changes may indicate phase transitions or structural rearrangements.

Density

- **Description:** Mass per unit volume of the system.
- **Importance:** Fundamental property reflecting the compactness or sparsity of molecules. Maintaining equilibrium density is crucial for accurate simulations and system stability.

Total Energy

- **Description:** Sum of kinetic and potential energies of all particles in the system.
- **Importance:** Conserved quantity in isolated systems. Monitoring total energy ensures simulation stability and accuracy. Sudden changes may indicate issues such as numerical instability.

Total Potential Energy

- **Description:** Energy associated with potential interactions between particles.
- **Importance:** Provides insights into intermolecular forces and interactions. Changes in potential energy indicate structural changes, phase transitions, or deviations from equilibrium.

2.1.1. Butanone

According to experimental values, the density of the butanone is $\rho = 800\ \mathrm{kg\,m^{-3}}$

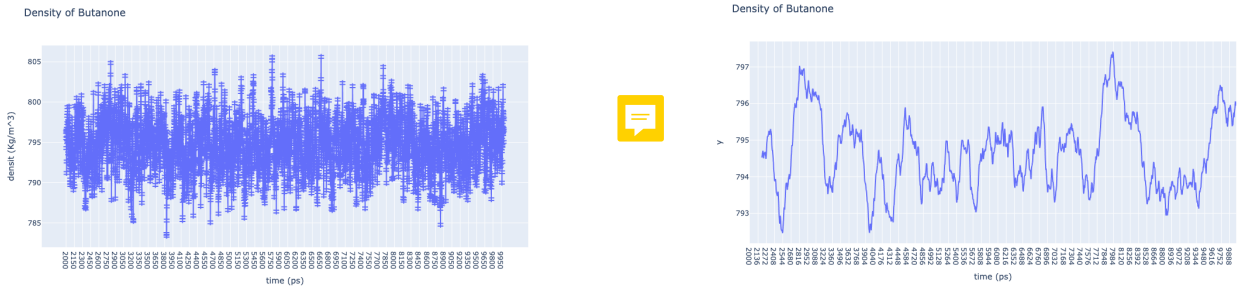

(a) Density of Butanone considering error

(b) Density of Butanone with moving average W = 100, unit: kg/m^3

Figure 5: Representation of Density of Butanone

RMSD	Error (Confidence Interval)	Mean
3.23966134	0.166647638	794.64665710775

Table 1: Description of RMSD, Error and Mean defined in $\mathrm{kg\,m^{-3}}$

Compared to the experimental value, the computational value found was lower than the experimental one

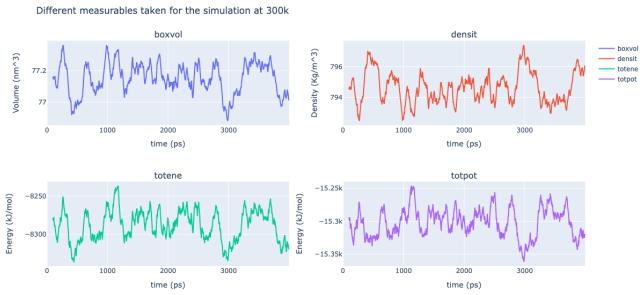

Figure 6: Different measurables taken for the simulation at 300k

2.1.2. 3-Hexanone

According to experimental values, the density of the 3-Hexanone is $\rho = 815\ \mathrm{kg\,m^{-3}}$

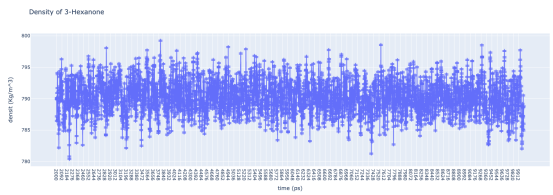

(a) Density of 3-Hexanone considering error

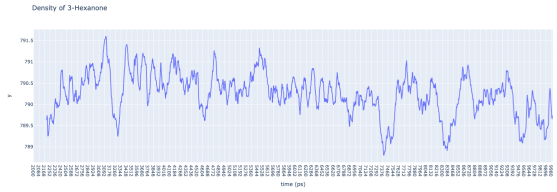

(b) Density of 3-Hexanone with moving average W = 100, unit: kg/m^3

Figure 7: Representation of Density of Butanone

RMSD	Error (Confidence interval)	Mean
2.5998717	0.0890240042	790.233328

Table 2: Description of RMSD, Error, and Mean defined in $\mathrm{kg\,m^{-3}}$

Compared to the experimental value, the computational value found was significantly lower than the experimental one.

2.1.3. *Comparison & General Considerations*

We can notice that the simulation was better at describing the density of the Butanone ($|exp.val - sim.mean| \approx 5.5 kg/m^3$) with respect to the Hexanone ($|exp.val - sim.mean| \approx 24.8 kg/m^3$)

2.2. *Heat of Vaporization*

The following step focused on the calculation of the Heat of Vaporisation. The molar heat of vaporization represents the enthalpy change associated with transferring one mole of the substance from its pure liquid state to the hypothetical gas phase, considering a specific temperature and pressure. This value can be computed by analyzing our liquid-phase simulations conducted at 300 K and 1 bar through the equation $\Delta H_{\mathrm{vap}} = U_{\mathrm{gas}} - U_{\mathrm{liq}} + RT + \Delta_{\mathrm{QM}} H_{\mathrm{Hvap}}$

2.2.1. *Butanone*

Given the average values: $U_{\mathrm{gas}} = 3.54\mathrm{kJ\,mol^{-1}}$ $U_{\mathrm{liq}} = -29.88\mathrm{kJ\,mol^{-1}}$ $RT = 2494.2\mathrm{kJ\,mol^{-1}}$
We obtain
$\Delta_{\mathrm{QM}} H_{\mathrm{vap}} = 35.92 \pm 0.01\mathrm{kJ\,mol^{-1}}$

According to experimental results, $\Delta_{\mathrm{QM}} H_{\mathrm{vap}} = 34.5\mathrm{kJ\,mol^{-1}}$. In this case, the computational value is higher than what can be calculated with experiments.

The calculated values exhibit dynamic behavior, predominantly representing average tendencies. Notably, there is observable variation over time, as illustrated by changes, such as those seen in the heat vaporization values.

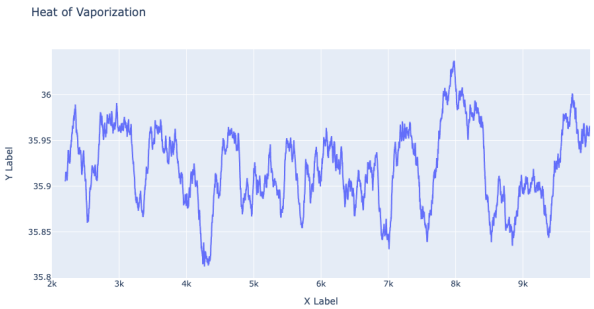

Figure 8: Heat Vaporisation over time with moving average W = 100

2.2.2. 3-Hexanone

Given the average values: $U_{gas} = 7.06 kJ\,mol^{-1}$ $U_{liq} = -34.67 kJ\,mol^{-1}$ $RT = 2494.2 kJ\,mol^{-1}$
We obtain
$\Delta_{QM}H_{vap} = 44.22 \pm 0.01 kJ\,mol^{-1}$

According to experimental results, $\Delta_{QM}H_{vap} = 42.5 kJ\,mol^{-1}$. In this case, the computational value is again higher than what can be calculated with experiments.

2.2.3. Comparison & General Considerations

This time we can notice that the simulation of the 3-Hexanone did a better job at reproducing the experimental data with respect to the butanone.($|exp.val - sim.mean| \approx 1.4 KJmol^{-1}$) for the butanone and ($|exp.val - sim.mean| \approx 1.7 KJmol^{-1}$) for the 3-hexanone

2.2.4. Further Discussion

TQ1) When calculating H_{vap} there is an approximation given the molar volume of the liquid is negligible compared to the gas state Step 1: Calculate the molar volume of the liquid

The molar volume of a liquid is given by the following equation:

$$V_{liq} = \frac{M}{\rho}$$

where:

V_{liq} is the molar volume of the liquid in m^3/mol
M is the molar mass of the compound in g/mol
ρ is the density of the liquid in kg/m^3

We are given that the density of propanone is 784 kg/m³ and the molar mass of propanone is 58.12 g/mol. Plugging these values into the equation, we get:

$$V_{liq} = \frac{(58.12 \text{ g/mol})}{(784 \text{ kg/m}^3)} = 0.0000741 \text{ m}^3\text{/mol}$$

Step 2: Calculate the molar volume of an ideal gas

The molar volume of an ideal gas is given by the following equation:

$$V_{gas} = \frac{RT}{P}$$

where:

V_{gas} is the molar volume of the gas in m^3/mol
R is the gas constant in J/(mol·K)
T is the temperature in K
P is the pressure in bar

"We are given that the temperature is 300 K and the pressure is 1 bar. The gas constant is 8.314 J/(mol·K). Plugging these values into the equation, we get:

$$V_{gas} = \frac{(8.314 \text{ J/(mol·K)})}{(100{,}000 \text{ Pa})} \cdot (300 \text{ K}) \approx 0.00249 \text{ m}^3\text{/mol}$$

Step 3: Calculate the error

The error in the approximation that the molar volume of a liquid is negligible compared to that of an ideal gas is given by the following equation:

$$\text{error} = P \cdot V_{liq}$$

where:

error is the error in $Pa \cdot m^3/mol$

P is the pressure in Pa

V_{liq} is the molar volume of the liquid in m^3/mol

Plugging in the values we calculated in Steps 1 and 2, we get:

$$\text{error} = (100,000 \text{ Pa}) \cdot (0.0000741 \text{ m}^3/\text{mol}) = 7.41 \text{ Pa} \cdot \text{m}^3/\text{mol}$$

Step 4: Convert the error to Pa·L/mol

To convert the error from Pa·m³/mol to Pa·L/mol, we multiply by 1000:

$$\text{error} = (7.41 \text{ Pa} \cdot \text{m}^3/\text{mol}) \cdot (1000 \text{ L/m}^3) = 7410 \text{ Pa} \cdot \text{L/mol}$$

Conclusion

The error in the approximation that the molar volume of a liquid is negligible compared to that of an ideal gas for the compound propanone at 300 K and 1 bar is 7410 Pa·L/mol."

TQ3) classical molecular dynamics (MD) simulations can be used to extract the molar heat of formation (ΔH_f) of a liquid. MD simulations are a computational method that can simulate the behavior of atoms and molecules at the atomic level, providing insights into various thermodynamic properties.

To calculate ΔH_f using MD simulations, the following steps are typically performed:

1. Create a simulation box containing a representative number of atoms or molecules of the liquid.
2. Assign initial positions and velocities to the atoms or molecules in the simulation box.
3. Simulate the interactions between the atoms or molecules using a classical force field.
4. Calculate the average potential energy of the system over the course of the simulation.

The molar heat of formation can then be calculated using the following equation:

$$\Delta H_f = E_{\text{potential}} - E_{\text{reference}}$$

where:

ΔH_f is the molar heat of formation in J/mol

$E_{\text{potential}}$ is the average potential energy of the system in J

$E_{\text{reference}}$ is the average potential energy of the system when the atoms or molecules are in their standard states in J

MD simulations have been successfully employed to calculate ΔH_f for various liquids, including water, methane, and ethanol. The results of these simulations have demonstrated good agreement with experimental data.

In addition to calculating ΔH_f, MD simulations can also be utilized to compute other thermodynamic properties of liquids, such as the molar heat capacity (C_P) and the molar entropy (S). These properties can be determined by monitoring the fluctuations of potential energy, volume, and temperature during the simulation.

Overall, MD simulations serve as a powerful tool for calculating a variety of thermodynamic properties of liquids, encompassing ΔH_f, C_P, and S.

2.3. Molar Isochoric Heat Capacity

The molar isochoric heat capacity represents the amount of heat required to be transferred to one mole of a substance to increase its temperature by 1 K under constant-volume conditions. The determination of the molar isochoric heat capacity involves performing three NVT simulations at temperatures of 290 K, 300 K, and 310 K. These simulations enable the assessment of how the heat capacity changes with temperature under constant-volume conditions for the considered liquids.

$$c_V = \frac{1}{N}\frac{\partial E}{\partial T} \approx \frac{1}{N}\frac{U(T_1) - U(T_0)}{T_1 - T_0} + \alpha R + \Delta_{\mathrm{QM}} c_{\mathrm{v}}$$

2.3.1. Butanone

The experimental heat capacity is given by $0.127 KJmol^{-1}K^{-1}$

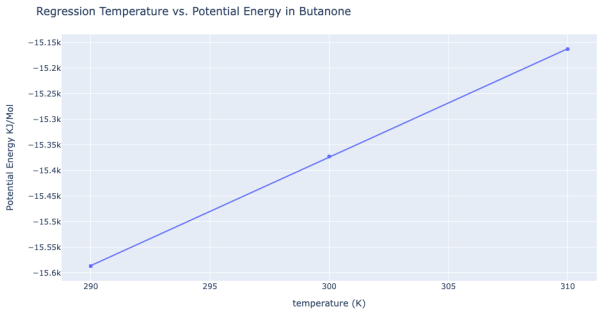

Figure 9: Linear Regression for estimating $\frac{\partial U(T)}{\partial T}$

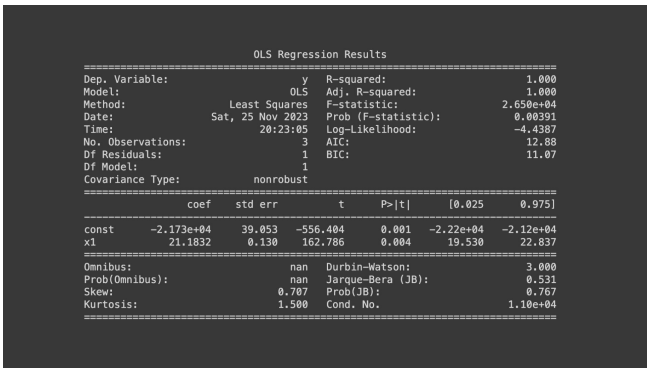

OLS Regression Results

Dep. Variable:	y	R-squared:	1.000
Model:	OLS	Adj. R-squared:	1.000
Method:	Least Squares	F-statistic:	2.650e+04
Date:	Sat, 25 Nov 2023	Prob (F-statistic):	0.00391
Time:	20:23:05	Log-Likelihood:	−4.4387
No. Observations:	3	AIC:	12.88
Df Residuals:	1	BIC:	11.07
Df Model:	1		
Covariance Type:	nonrobust		

	coef	std err	t	P>|t|	[0.025	0.975]
const	−2.173e+04	39.053	−556.404	0.001	−2.22e+04	−2.12e+04
x1	21.1832	0.130	162.786	0.004	19.530	22.837

Omnibus:	nan	Durbin-Watson:	3.000
Prob(Omnibus):	nan	Jarque-Bera (JB):	0.531
Skew:	0.707	Prob(JB):	0.767
Kurtosis:	1.500	Cond. No.	1.10e+04

Figure 10: OLS Regression Results

Table 3: Regression Coefficients

Parameter	Value
Slope	21.18319999999981 kJ $\mathrm{mol}^{-1}\,\mathrm{K}^{-1}$
Value of α	5.5
c_{v}	0.10860298189899964 kJ $\mathrm{mol}^{-1}\,\mathrm{K}^{-1}$

2.3.2. 3-Hexanone

The experimental heat capacity is given by $0.217 KJmol^{-1}K^{-1}$

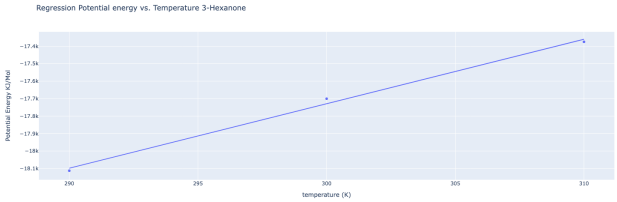

Figure 11: Linear Regression for estimating $\frac{\partial U(T)}{\partial T}$

OLS Regression Results

Dep. Variable:	y	R-squared:	0.995
Model:	OLS	Adj. R-squared:	0.991
Method:	Least Squares	F-statistic:	217.8
Date:	Tue, 14 Nov 2023	Prob (F-statistic):	0.0431
Time:	14:14:13	Log-Likelihood:	-13.306
No. Observations:	3	AIC:	30.61
Df Residuals:	1	BIC:	28.81
Df Model:	1		
Covariance Type:	nonrobust		

	coef	std err	t	P>|t|	[0.025	0.975]
const	-2.88e+04	750.428	-38.378	0.017	-3.83e+04	-1.93e+04
x1	36.9024	2.501	14.758	0.043	5.130	68.674

Omnibus:	nan	Durbin-Watson:	3.000
Prob(Omnibus):	nan	Jarque-Bera (JB):	0.531
Skew:	0.707	Prob(JB):	0.767
Kurtosis:	1.500	Cond. No.	1.10e+04

Figure 12: OLS Regression Results

Table 4: Regression Coefficients

Parameter	**Value**
Slope	$36.90236499999974\ \text{kJ mol}^{-1}\,\text{K}^{-1}$
Value of α	7.5
c_{v}	$0.1655334012756245\ \text{kJ mol}^{-1}\,\text{K}^{-1}$

2.3.3. Comparison & General Considerations

We can notice that the computational value of heat capacity is lower than the experimental value either in the case of Butanone, or 3-Hexanone The value of the heat capacity for the 3-Hexanone is considerably ($\approx 23.8\%$ less) than the experimentally measured value.

2.3.4. Additional Remarks

TQ2) I would expect the molar isobaric heat capacity (C_P) to differ significantly from the molar isochoric heat capacity (C_V) for a given substance. This is because C_P and C_V are measures of two different heat capacities, and these heat capacities are related to the different ways in which energy can be transferred to a substance.

C_P is the heat capacity at constant pressure, which means that the pressure of the substance is held constant while heat is added. C_V is the heat capacity at constant volume, which means that the volume of the substance is held constant while heat is added.

When heat is added to a substance at constant pressure, the substance can expand, which means that its volume increases. This expansion can do work on the surroundings, so some of the heat that is added to the substance is used to do this work. As a result, C_P is always greater than C_V for a given substance.

The difference between C_P and C_V is related to the work that is done on the surroundings during the heating process. For a substance that expands when heated at constant pressure, more work is done on the surroundings, so C_P is larger than C_V. For a substance that contracts when heated at constant pressure, less work is done on the surroundings, so C_P is smaller than C_V.

In general, the difference between C_P and C_V is larger for gases than for liquids or solids. This is because gases are more compressible than liquids or solids, so they can expand more when heated at constant pressure. As a result, the work done on the surroundings by a gas during heating is larger than the work done on the surroundings by a liquid or solid, so C_P is larger than C_V for gases.

2.4. Radial Distribution Function and Coordination Number

The radial distribution function (RDF) $g_{IJ}(r)$ serves as a metric for the local density of atoms of type I at a specific distance r from atoms of type J, relative to the bulk density of atoms of type J. This function is designed to be zero at $r = 0nm$ (as atoms cannot overlap) and tends towards one at large distances, reflecting bulk behavior.

In the liquid state, the RDF typically exhibits a sudden rise from zero, followed by successive peaks of decreasing magnitudes. These peaks correspond to shells of excess density at favorable interatomic distances, with the first peak often indicating the contact distance. Subsequently, the RDF levels off to approach a value of one.

2.4.1. Butanone

We first report the requested visualization for the **Carbonyl Oxygen - Carbonyl Carbon** case

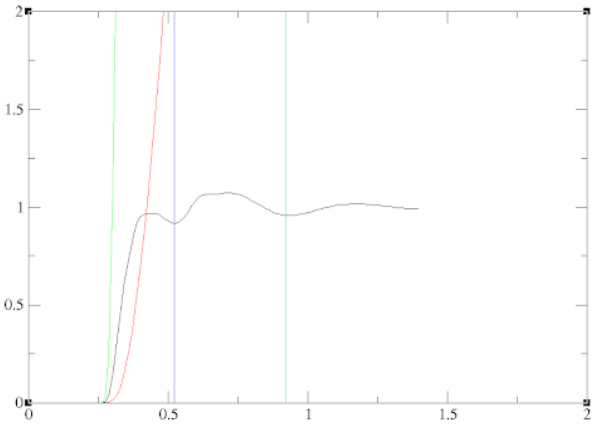

Figure 13: XMGRACE plots for O-C. Black: $g_{O,C}(r)$, Green: $\rho_C 4\pi r^2 g(r)$, Red: integral of $G(r) = \rho_C \int_0^R 4\pi r^2 g(r)$, Blue: first local minimum, Turquoise: second local minimum

As suggested in the assignment, in order to understand the coordination number we need to look at the value of $G(r)$) in correspondence with the local minima of $g(r)$. To do that we graphically see the intersection of the red curve with the vertical blue and turquoise curves.

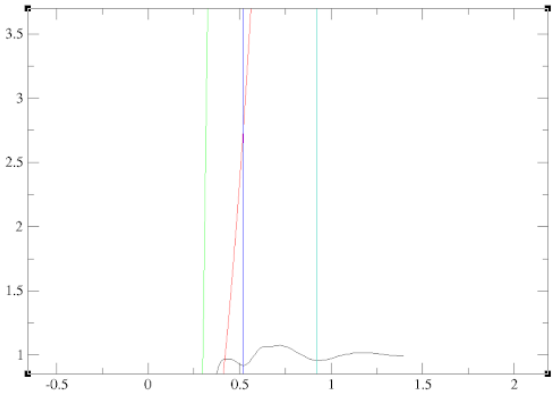

(a) Value of the integral at the first minimum

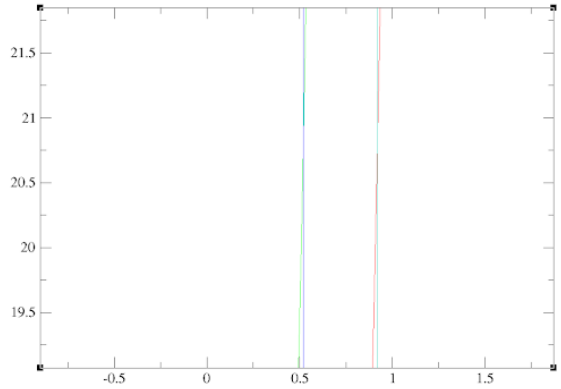

(b) Value of the integral at the second intersection

Figure 14: Value of the integral at first and second intersecitons

We see that for the first minimum corresponds a value of $\approx 2.75nm$ and for the second minimum a value of $\approx 21.8nm$

Now we turn our attention to the **Carbonyl Oxygen - Carbonyl Oxygen** case

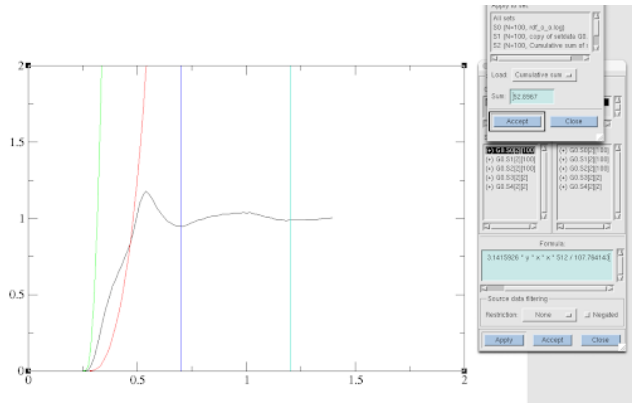

Figure 15: XMGRACE plots for O-C. Black: $g_{O,C}(r)$, Green: $\rho_C 4\pi r^2 g(r)$, Red: integral of $G(r) = \rho_C \int_0^R 4\pi r^2 g(r)$, Blue: first local minimum, Turquoise: second local minimum

Once again, in order to understand the coordination number we need to look at the value of $G(r))$ in correspondence with the local minima of $g(r)$. To do that we graphically see the intersection of the red curve with the vertical blue and turquoise curves.

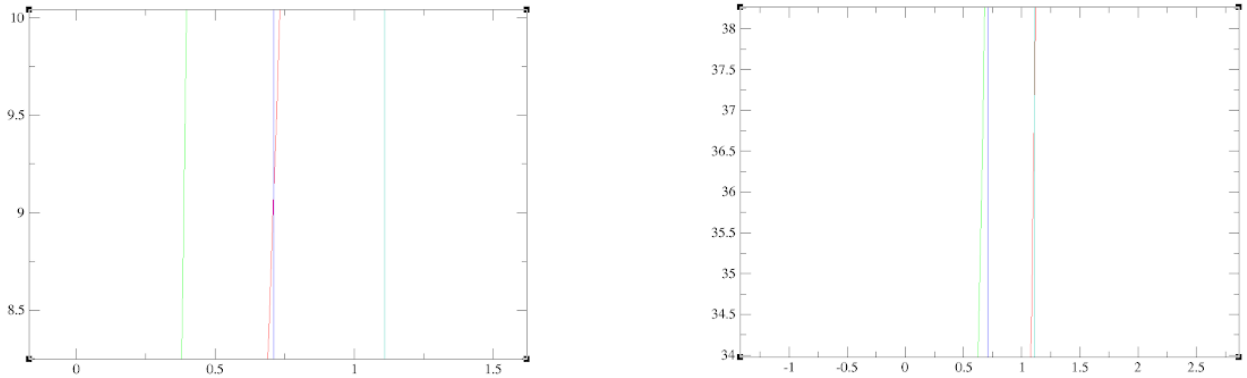

(a) Value of the integral at the first minimum

(b) Value of the integral at the second intersection

Figure 16: Value of the integral at first and second intersecitons

We see that for the first minimum corresponds a value of $\approx 9.11nm$ and for the second minimum a value of $\approx 36.9nm$

2.4.2. 3-Hexanone

We first report the requested visualization for the **Carbonyl Oxygen - Carbonyl Carbon** case

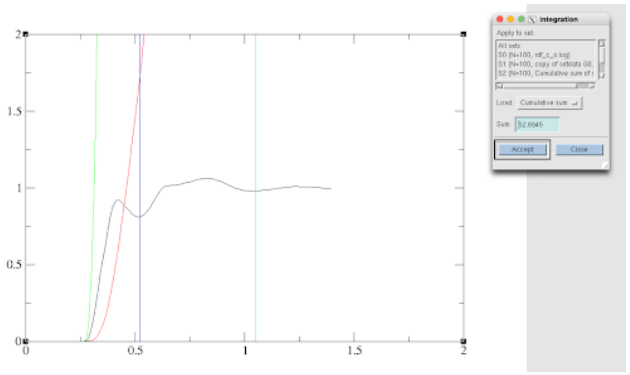

Figure 17: XMGRACE plots for O-C. Black: $g_{O,C}(r)$, Green: $\rho_C 4\pi r^2 g(r)$, Red: integral of $G(r) = \rho_C \int_0^R 4\pi r^2 g(r)$, Blue: first local minimum, Turquoise: second local minimum

As suggested in the assignment, in order to understand the coordination number we need to look at the value of $G(r)$) in correspondence with the local minima of $g(r)$. To do that we graphically see the intersection of the red curve with the vertical blue and turquoise curves.

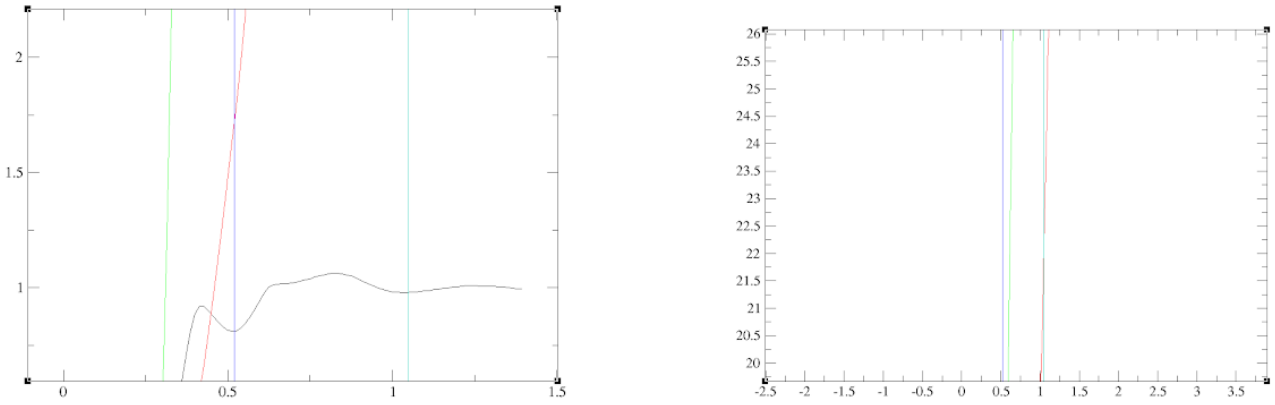

(a) Value of the integral at the first minimum

(b) Value of the integral at the second intersection

Figure 18: Value of the integral at first and second intersecitons

We see that for the first minimum corresponds a value of $\approx 1.75nm$ and for the second minimum a value of $\approx 22.0nm$

Now we turn our attention to the **Carbonyl Oxygen - Carbonyl Oxygen** case

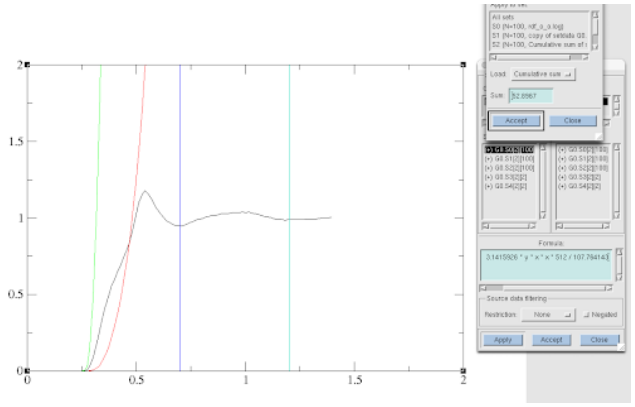

Figure 19: XMGRACE plots for O-C. Black: $g_{O,C}(r)$, Green: $\rho_C 4\pi r^2 g(r)$, Red: integral of $G(r) = \rho_C \int_0^R 4\pi r^2 g(r)$, Blue: first local minimum, Turquoise: second local minimum

Once again, in order to understand the coordination number we need to look at the value of $G(r)$) in correspondence with the local minima of $g(r)$. To do that we graphically see the intersection of the red curve with the vertical blue and turquoise curves.

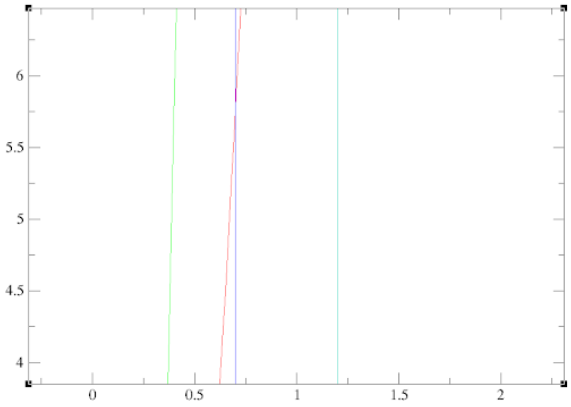

(a) Value of the integral at the first minimum

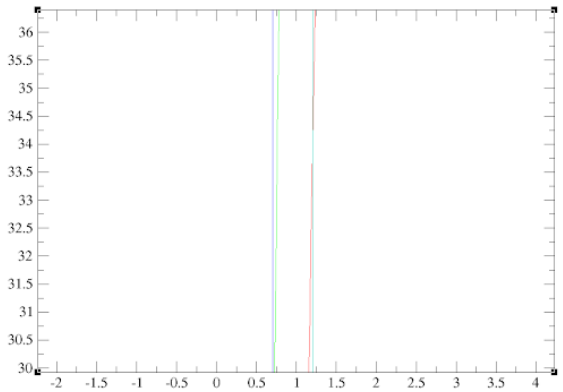

(b) Value of the integral at the second intersection

Figure 20: Value of the integral at first and second intersecitons

We see that for the first minimum corresponds a value of $\approx 5.75nm$ and for the second minimum a value of $\approx 34.0nm$

2.4.3. Comparison & General Considerations

When comparing the two molecules we notice that the values obtained for the coordination number when considering C-O are very close with respect to these values when considering O-O.

In both cases, we noticed how the first local minimum of $g_{I,J}(r)$ s.t. $I = O$, $J = \{C, O\}$ was much more pronounced than the second.

2.5. Static Dieletric Permitivity

The static relative dielectric permittivity (ε) of a liquid is a crucial parameter that characterizes its ability to screen electrostatic interactions. This property becomes particularly significant in scenarios such as being placed between capacitor plates or between ions embedded within the liquid.

The evaluation of ε involves conducting a simulation of the pure liquid, focusing on the fluctuations of the total dipole moment within the computational box. When employing the reaction-field method to handle electrostatic interactions, incorporating a reaction-field permittivity ($\varepsilon_{\mathrm{RF}}$), the relevant equation takes the form of a Kirkwood-Fröhlich type equation.

2.5.1. *Butanone*

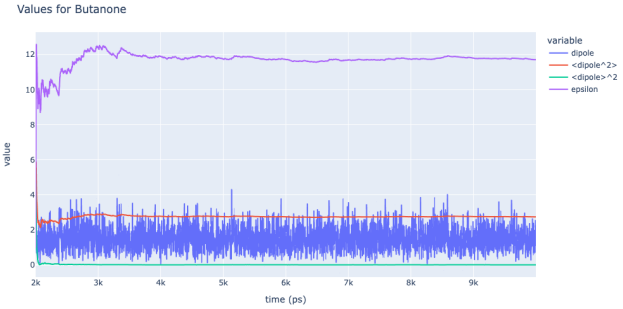

Figure 21: Values for Butanone

Here The mean on the second half of the simulation The standard devition on the second half of the simulation

Metric	Value
Mean	11.739
Standard Deviation	0.073

2.5.2. *3-Hexanone*

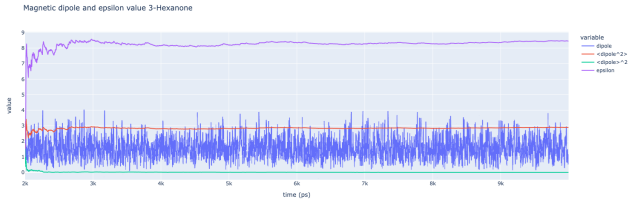

Figure 22: Values for $3_H exanone$

Here The mean on the second half of the simulation The standard devition on the second half of the simulation

Metric	Value
Mean	8.339
Standard Deviation	0.067

2.5.3. *Comparison & General Considerations*

We can notice how the value of ε for 3-Hexanone is much lower ($\approx 28.96\%$) than the one of Butanone

2.6. *Self-Diffusion Coefficient*

The self-diffusion coefficient is a fundamental parameter that quantifies the rate at which individual particles within a substance move through the medium on their own accord. It characterizes the diffusion of particles within the substance without external influences. In the context of molecular dynamics simulations or experimental studies, the self-diffusion coefficient provides insights into the mobility and dynamics of individual particles, reflecting the inherent properties of the substance.

2.6.1. *Butanone*

The Diffusion coefficient was found to be linear and dependent on time. For this reason, it was possible to fit values using $D = 0.00355405 nm^2 / ps$ & $R^2 = 0.999672$

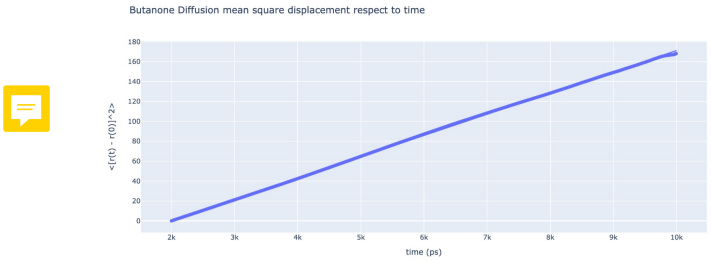

Figure 23: Diffusion mean square displacement of Butanone respect to time

2.6.2. 3-Hexanone

Also in this setting, the Diffusion coefficient was found to be linear and dependent on time. For this reason, it was possible to fit values using $D = 0.00257262 nm^2 / ps$ & $R^2 = 0.999818$

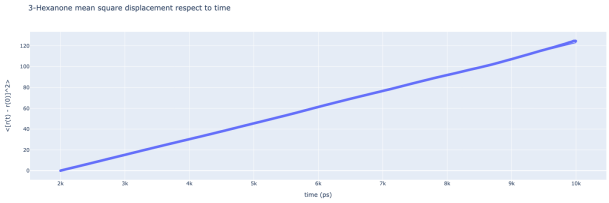

Figure 24: Diffusion mean square displacement of 3-Hexanone respect to time

2.6.3. Comparison & General Considerations

We can observe that the diffusion coefficient of the Butanone is higher ($\approx 29.26\%$) than the one of he 3-Hexanone. We underline that the fitted line of the two scatterplot is present, but it looks indistinguishable form the point because of the goodness fo the fit.

2.7. Final Considerations

TQ4) GROMOS employs diverse methodologies to enhance transferability, encompassing the following strategies:

1. **Parameter Fitting:** The force field parameters pertaining to various molecular types undergo fitting against corresponding experimental data. This ensures precise replication of individual molecule properties within the force field. GROMOS utilizes multiple forms of experimental data, encompassing molecular structure, thermodynamics, and dynamics, to optimize force field parameters through a variety of optimization algorithms.

2. **Combination Rules:** Interaction between different atom types is computed using combining rules grounded in physical atom properties, such as size and electronegativity. GROMOS employs a spectrum of combining rules based on the well-established Lennard-Jones potential to determine interactions between distinct atom types.

3. **Charge Assignment:** Atom charges within molecules are computed using diverse methods, including the RESP method. These charges are crucial for calculating electrostatic interactions. GROMOS utilizes various techniques for charge assignment, including the RESP method, which determines charges based on the molecule's electrostatic potential.

Through the implementation of these techniques, GROMOS achieves a high level of transferability, even in instances lacking experimental data for cross-interactions. This capability enables GROMOS to simulate a broad range of systems, including mixtures of diverse molecule types.

However, it is essential to acknowledge that transferability is not flawless, and some error in cross-interaction calculations is inevitable. This discrepancy may be particularly pronounced in mixtures of highly dissimilar molecules. Consequently, validating GROMOS simulation results with experimental data is imperative.

Additional insights into the specific techniques employed by GROMOS to attain transferability are provided below:

In summary, GROMOS stands out as a potent tool for simulating diverse systems. Nevertheless, the precision of GROMOS simulations hinges on the force field's transferability, underscoring the need for rigorous validation against experimental data whenever feasible.

3. Appendix

Summary 1

You can find the list for the Google Colab Jupyter here.

References

[1] Y. He, Y. Chen, P. Alexander, P. N. Bryan, J. Orban, Nmr structures of two designed proteins with high sequence identity but different fold and function, Proceedings of the National Academy of Sciences 105 (2008) 14412–14417.

[2] J. R. Allison, M. Bergeler, N. Hansen, W. F. van Gunsteren, Current computer modeling cannot explain why two highly similar sequences fold into different structures, Biochemistry 50 (2011) 10965–10973.